





Article

Synthesis of Novel MOF-5 Based BiCoO₃ Photocatalyst for the Treatment of Textile Wastewater

Bazla Sarwar ¹, Asad Ullah Khan ^{1,2,*}, Tahir Fazal ³ , Muhammad Aslam ¹ , Naeem Akhtar Qaisrani ³  and Ashfaq Ahmed ^{4,*} 

¹ Department of Chemical Engineering, COMSATS University Islamabad, Lahore Campus, Lahore 54000, Pakistan

² Department of Chemical Engineering, SCME, National University of Sciences and Technology (NUST), Sector H12, Islamabad 44000, Pakistan

³ Institute of Chemical and Environmental Engineering (ICEE), Khwaja Fareed University of Engineering and Information Technology, Rahim Yar Khan 64200, Pakistan

⁴ Institute for Sustainable Industries and Liveable Cities, Victoria University, Melbourne 8001, Australia

* Correspondence: asad.khan@scme.nust.edu.pk (A.U.K.); ashfaq.ahmed@vu.edu.au (A.A.)

Abstract: Water pollution, having organic dyes, has lethal impacts on aquatic life and public health. To eliminate or degrade dyes, a metal-organic framework (MOF) based BiCoO₃ semiconductor is considered a potential photocatalyst for the degradation of dyes. In this study, the MOF-5-based BiCoO₃ (MOF-5/BiCoO₃) composite was successfully synthesized using a one-pot hydrothermal process. Different analytical techniques were used to characterize MOF-5/BiCoO₃ composite and pure MOF-5 samples. When compared to pure MOF-5, the experimental and characterization analysis showed that the MOF-5/BiCoO₃ composite has better photocatalytic activity (99.6%) for the degradation of Congo-red (CR) dye due to the formation of heterostructure between MOF-5 and BiCoO₃, which improve the separation of charge carriers. Meanwhile, the introduction of BiCoO₃ with MOF-5 changes the surface morphology of MOF-5/BiCoO₃ composite, increasing the surface area for CR adsorption and thus improving photocatalytic efficiency. Based on radical trapping experiments, the superoxide and hydroxyl radicals are dominant species in the CR degradation process. The reusability results demonstrate that MOF-5/BiCoO₃ composite can be used effectively for up to five cycles, which makes the process more economical. Hence, MOF-5/BiCoO₃ composite offers a promising approach to developing a highly effective, stable, efficient, economical, and sustainable photocatalyst for the dissociation of organic pollutants from wastewater streams.

Keywords: textile wastewater; MOF-5; BiCoO₃ semiconductor; Congo-red dye; photocatalysis



Citation: Sarwar, B.; Khan, A.U.; Fazal, T.; Aslam, M.; Qaisrani, N.A.; Ahmed, A. Synthesis of Novel MOF-5 Based BiCoO₃ Photocatalyst for the Treatment of Textile Wastewater. *Sustainability* **2022**, *14*, 12885. <https://doi.org/10.3390/su141912885>

Academic Editor: Haibing Tang

Received: 4 August 2022

Accepted: 30 September 2022

Published: 9 October 2022

Publisher's Note: MDPI stays neutral with regard to jurisdictional claims in published maps and institutional affiliations.



Copyright: © 2022 by the authors. Licensee MDPI, Basel, Switzerland. This article is an open access article distributed under the terms and conditions of the Creative Commons Attribution (CC BY) license (<https://creativecommons.org/licenses/by/4.0/>).

1. Introduction

Water pollution, generated mainly by industrial, domestic, and agricultural activities, becomes a major environmental issue [1–3]. In particular, the textile industry releases a large volume of wastewater, containing auxiliary substances and organic dyes, into water bodies [4,5], which leads the aquatic environment to pollution and aquatic diseases [6,7]. To tackle this wastewater, photocatalysis, an advanced oxidation process, is widely used to eliminate or degrade the organic dyes from textile wastewater [8,9]. Semiconductor photocatalysts have received a lot of interest in the last two decades because of their ability to use solar energy to reduce the growing environmental degradation [10].

Many semiconductor photocatalysts such as TiO₂, ZnO, Fe₂O₃, CuO, and BiVO₄ have been employed to treat organic pollutants from wastewater [9,11–13]. Among them, TiO₂, as a first-generation semiconductor photocatalyst, has piqued the interest of many researchers because of its good photocatalytic efficiency, nontoxicity, stability, low cost, and ease of preparation [14]. However, the utilization of TiO₂ photocatalysts is restricted in wastewater treatment application for reasons including: its low porosity, low specific surface area, poor

adsorption capability, difficult recovery, wider band gap defects, fast recombination of charge carriers, and only utilize ultraviolet (UV) light from sunlight [15–18]. Therefore, developing a semiconductor that has a slower recombination of charge carriers, lower band gap, and better light absorption under UV-visible region is necessary to replace TiO_2 photocatalyst.

Recently, metal-organic frameworks (MOFs), developed as functionalized metal-organic hybrid materials, are considered promising materials due to their applications in the adsorption of pollutants and photocatalysis [19,20]. MOFs (i.e., MOF-5) offer higher specific surface area, a well-organized porous structure, better hydrothermal stability, and tunable organic metal clusters or organic linkers characteristics [15,21]. However, MOF-5 has limited adsorption capacity, fast electron-hole recombination process, wide energy band gap (3.88 eV), and poor light absorption under the visible light region, which limits its application in wastewater treatment [19,22]. To overcome the MOFs related barriers, MOF-5 can be integrated with the aid of rare metal ions and/or semiconductors to modify MOFs as an efficient heterogeneous semiconductor, as it can act as a carrier transmission route due to its open metal sites, unsaturated metal cores, and catalytically active organic linkers [21]. MOF-based semiconductors can promote the generation and separation of photoexcited charge carriers along with a high capability to uptake solar energy and enhanced photocatalytic activity to degrade the organic dyes [23].

In this context, multiferroics materials (i.e., Bi_2WO_6 , BiFeO_3 , and BiCoO_3) have been used in multiple applications such as catalysis, photocatalysis, and electrochemistry [22,24–26]. BiCoO_3 provides significant properties including tetragonal structure, spontaneous polarization, smaller band gap (2.2 eV), and good response in the UV-visible light region, which improves its photocatalytic performance as compared to TiO_2 photocatalyst [27]. Depending on these factors, the use of BiCoO_3 as a semiconductor with MOFs is a substantial piece of work. Pristine MOF-5, Zn_4O -based MOF, offers physical and chemical advantages (as mentioned above) for the synthesis of MOF-5-based BiCoO_3 heterogeneous photocatalysts, [17,28]. Hence, modified MOFs (MOF-5-based BiCoO_3) can be used as an efficient, effective, and stable heterogeneous photocatalyst, which can provide better intrinsic properties such as higher surface area, higher adsorption capacity, higher separation of charge carriers, and good response in visible light absorption than pure MOFs. According to the literature, no study has been reported on the modification of MOF-5 with the loading of BiCoO_3 semiconductors for the removal of organic dyes.

The focus of this study was to synthesize an efficient and effective MOF-5-based semiconductor for the photocatalytic degradation of organic dyes from simulated textile wastewater. For this purpose, MOF-5 material was modified with the loading of BiCoO_3 semiconductor. The as-prepared samples of MOF-5 (as control) and MOF-5/ BiCoO_3 composite were characterized to evaluate their intrinsic properties such as crystallinity, specific surface area, morphology, functional groups, and recombination of charge carriers. The as-prepared samples were utilized to investigate their photocatalytic performance for the degradation of Congo-red dye. The MOF-5/ BiCoO_3 composite was used to investigate the role of radicals and reusability of the sample for the degradation of dye molecules.

2. Materials and Methods

2.1. Chemicals and Reagents

The precursors used in this experiment are: zinc acetate dihydrate ($\text{Zn}(\text{CH}_3\text{COO})_2 \cdot 2\text{H}_2\text{O}$) as zinc precursor, terephthalic acid ($\text{C}_6\text{H}_4(\text{CO}_2\text{H})_2$) as organic ligand, triethylamine ($\text{N}(\text{CH}_2\text{CH}_3)_3$) as a capping agent, N, N-dimethylformamide ($\text{C}_3\text{H}_7\text{NO}$, DMF) as a solvent, cobalt nitrate ($\text{Co}(\text{NO}_3)_2 \cdot 9\text{H}_2\text{O}$), bismuth nitrate ($\text{Bi}(\text{NO}_3)_3 \cdot 5\text{H}_2\text{O}$), polyethylene glycol (PEG-2000), potassium hydroxide (KOH), and nitric acid (HNO_3). These chemicals were procured from Merck (Germany) to prepare MOF-5 and MOF-5/ BiCoO_3 composite. The model dye i.e., Congo-red ($\text{C}_{32}\text{H}_{22}\text{N}_6\text{Na}_2\text{O}_6\text{S}_2$) was purchased from Sigma Aldrich for the photocatalytic degradation experiment. Triethanolamine (TEOA), isopropanol (IPA), and benzoquinone (BQ) agents are utilized in radical trapping experiments. Ultrapure water,

produced by the water purification unit (Adrona SIA-B30, Rīga, Latvia), was utilized to prepare all solutions during experiments.

2.2. Synthesis of MOF-5

The MOF-5 sample was prepared by solvothermal approach. Firstly, the organic solution was formed by the addition of 5.065 g terephthalic acid (30.5 mmol) as an organic linker and 8.5 mL of triethylamine as a capping agent in 400 mL of DMF solvent. Secondly, the 16.99 g (77.4 mmol) of zinc acetate dihydrate was added in a separate beaker, having 500 mL of DMF. This zinc metal solution was poured dropwise into the previous organic solution under 15 min time interval [29]. After combining both solutions, the mixture was stirred vigorously for 2 h to obtain white precipitates of MOF-5. The entire procedure was performed at ambient temperature with no additional heating. The precipitates of MOF-5 were separated using centrifugation, prior to washing three times using DMF. The obtained MOF-5 particles were dispersed again in 250 mL of DMF overnight. After that, particles were separated again by centrifugation process. The falcon tubes having whitish particles were placed in a drying oven at 60 °C for 24 h to obtain dry particles. Then, dried MOF-5 particles were collected in a closed vial until further use in the synthesis of modified MOF-5 material using BiCoO_3 .

2.3. Preparation of MOF-5/ BiCoO_3 Composite

The hydrothermal method was used to load BiCoO_3 nanoparticles on MOF-5 substrate, as it provides high purity, controllable morphology, and well-ordered particle size distribution during the preparation method. To make the MOF-5/ BiCoO_3 composite, cobalt nitrate and bismuth nitrate were mixed in ultrapure water in a 1:1 molar ratio. The 1 mL nitric acid (68 wt.%) and 2 g polyethylene glycol (PEG-2000) were mixed with the previous mixture under constant agitation at ambient conditions. To adjust the pH of the solution to neutral, KOH (1 M) solution was applied dropwise into the mixture as slowly as possible until the solution neutralized. The prepared solution was divided into two parts, one part was shifted directly into a Teflon-lined stainless autoclave to be placed in a heating oven for 24 h at 180 °C [30]. Afterward, 300 mg of the as-prepared MOF-5 sample was dispersed in the second part of the previous solution. For the preparation of the modified MOF-5/ BiCoO_3 composite, the solution of MOF-5 and BiCoO_3 was shifted to a 50 mL Teflon-lined stainless autoclave, and then the closed autoclave was placed in an oven to heat the mixture at 180 °C for 24 h, as shown in Figure 1. After cooling, the MOF-5/ BiCoO_3 precipitates were separated using centrifugation (9000 rpm, 5 min). The as-prepared MOF-5/ BiCoO_3 composite was rinsed with ultrapure water to remove any impurities or unreacted precursors. Finally, the as-prepared MOF-5/ BiCoO_3 composite was heated in an oven at 80 °C for 14 h to obtain dried MOF-5/ BiCoO_3 powder.

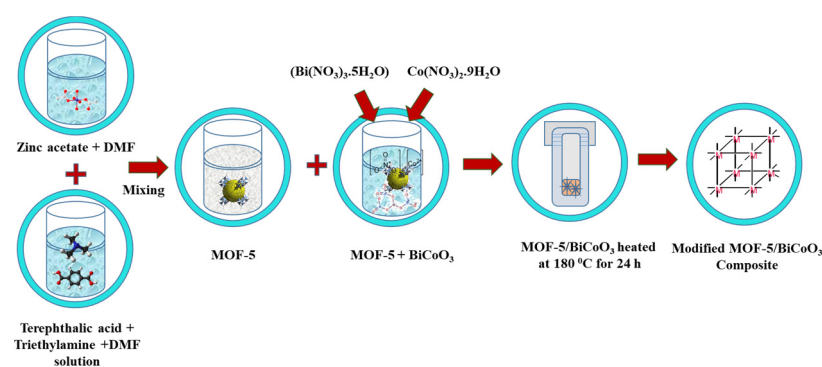


Figure 1. Synthesis route of modified MOF-5/ BiCoO_3 composite.

2.4. Characterization of Samples

The pure MOF-5 and modified MOF-5-based BiCoO_3 photocatalysts were characterized to investigate their intrinsic properties using different instrumental techniques. X-ray

diffraction (XRD) was carried out using an X-pert powder diffractogram instrument in the angular range of $2\theta = 10\text{--}70^\circ$ with Cu K α radiation and the scan speed of 1° min^{-1} , which identified the crystallinity of samples. The Brunauer-Emmett-Teller (BET, Micromeritics, Norcross, GA, USA) analyzer was used to determine the surface area and pore size of samples. Scanning electron microscopy (SEM, TESCAN Vega LMU) was carried out to study the microstructure and morphology of as-prepared samples. The functional groups of MOF-5 and MOF-5/BiCoO₃ samples were identified using Fourier transform infrared (FTIR, Perkin Elmer/Spectrum II) spectrometer using ATR disc mode in the range of $500\text{--}4000 \text{ cm}^{-1}$ wavenumber. The photoluminescence (PL) spectroscopy was carried out in the range of 200–900 nm to observe the recombination process of electron-hole pairs.

2.5. Photocatalytic Degradation Experiment

The photocatalytic degradation performance of samples was investigated in a batch mode using MOF-5 and MOF-5/BiCoO₃ composite. The aqueous solution of Congo-red (CR) dye was prepared and used as simulated textile wastewater without the addition of any chemical further. The stock solution of CR (1000 ppm) was prepared using 0.1 g of CR in 100 mL distilled water prior to the desired dilution (25 ppm). In photocatalytic degradation experiments, the 10 mg amount of photocatalyst was added to the photoreactor of 50 mL CR solution (having pH = 6 and 25 mg L^{-1} concentration). The suspension was stirred at 400 rpm for a specified contact time (30 min) under dark conditions for the achieving of adsorption/desorption equilibrium. For photocatalysis, the CR solution having photocatalyst is irradiated using a Xenon lamp (300 W), keeping the distance up to 5.5 cm between the source of light and photoreactor for the best illumination effect. Afterward, the 5 mL solution of CR was collected using a syringe and then centrifuged to separate the supernatant and photocatalyst during a 0–90 min time interval. The absorbance of CR solution was determined at 498 nm wavelength using a UV-Visible spectrometer (Bio base, Jinan, China) [5]. The remaining concentration of CR was measured using calibration curve ($Y = 0.0773X + 0.008$, $R^2 = 0.998$). Then, the photocatalytic degradation (%) was determined using Equation (1), whereas C_0 (mg L^{-1}) and C_t (mg L^{-1}) are the initial dye concentration and concentration at a predetermined time interval.

$$\text{Photocatalytic degradation (\%)} = \frac{C_0 - C_t}{C_0} \times 100 \quad (1)$$

The COD removal (%) was also measured to ensure the mineralization of CR dye. The initial and final values of COD were determined before and after photocatalytic degradation of CR dye using MOF-5, BiCoO₃, and MOF-5/BiCoO₃. Then, Equation (2) was used to determine COD removal (%). All experiments of photocatalytic degradation and COD test were performed in duplicates during this study.

$$\text{COD removal (\%)} = \frac{\text{COD}_{\text{initial}} - \text{COD}_{\text{final}}}{\text{COD}_{\text{initial}}} \times 100 \quad (2)$$

2.6. Role of Radical Trapping Scavengers

In the photocatalysis experiment, different radical scavengers were used to investigate their roles in the photocatalytic degradation process. Before the adsorption-desorption equilibrium stage, the active trapping agents such as BQ (5 mg), IPA (0.4 mL), and TEOA (0.1 mL) were poured into the solution under the same experimental conditions to trap the radicals of superoxide, hydroxyl, and holes, respectively.

2.7. Recycling of Photocatalyst

The recycling test was also performed for up to five cycles to observe the consistency of the sample in the photocatalytic degradation process. In this context, the photocatalyst was re-collected after the photocatalytic degradation of CR dye. Then, the photocatalyst

was washed three times with ultrapure water, prior to drying at 60 °C in an oven for 12 h. The dried samples were stored in closed vials until further use in the experiment.

3. Results and Discussion

3.1. Evaluation of Crystallinity, Morphological, Functional Groups, Specific Surface-Area, and Optical Properties of Prepared Samples

The XRD analysis of pristine MOF-5 and MOF-5/BiCoO₃ composite were investigated in the range of $2\theta = 5$ to 70° to observe the crystallinity. The XRD patterns of simulated and as-prepared samples are represented in Figure 2a–c. XRD pattern of MOF-5 revealed that the main peaks of the diffractogram appeared at $2\theta = 9.7^\circ$, 13.7° , and 15.4° corresponding to (220), (400), and (420) crystal planes, which confirm the formation of MOF-5 and aligned with a simulated one, see Figure 2a [31,32]. In addition, the small peaks of ZnO also appeared in the MOF-5 sample at 31.7° , 34.6° , 36.1° , and 47.5° , which are associated with the ZnO crystal planes of (100), (002), (101), and (102) [22,33]. The ZnO nanoparticles are trapped during the synthesis of MOF-5, as reported in the literature [31]. In simulated BiCoO₃ spectra, the crystal planes of 220, 010, 222, 021, 400, 411, and 611 appeared at the peaks of 24.8° , 27.8° , 30.4° , 33.2° , 35.1° , 36.4° , and 56.1° , which indicate the presence of Bi and Co oxides in nanoparticles [34], as given in Figure 2b. In MOF-based BiCoO₃, most of these peaks of MOF-5 are disappeared due to the addition of BiCoO₃ nanoparticles during the synthesis of the MOF-5/BiCoO₃ composite. The crystal planes of 220, 021, 411, and 611 for BiCoO₃ appeared at 24.8° , 33.2° , 36.4° , and 56.1° along with MOF-5 crystal planes (100, 002, and 101), which indicates that BiCoO₃ nanoparticles are well loaded on the surface of MOF-5 during the preparation of composite [27], as shown in Figure 2c.

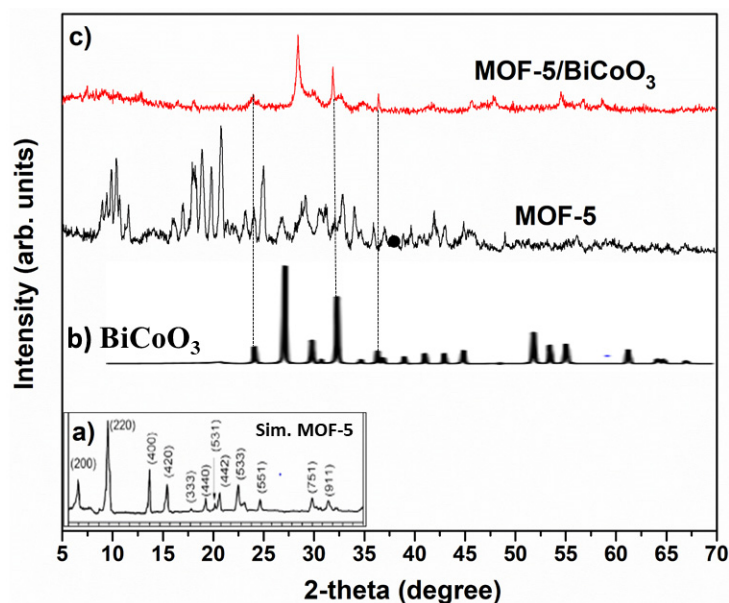


Figure 2. XRD of simulated MOF-5 (a); simulated BiCoO₃ (b); and as-synthesized MOF-5 and MOF-5/BiCoO₃ (c).

The prepared photocatalysts are examined using SEM-EDX analysis to study the morphology of samples. The SEM images of MOF-5, BiCoO₃, and MOF-5/BiCoO₃ composite are presented in Figure 3a–c. A large number of MOF-5 layers are formed during the synthesis process, which indicates that MOF-5 crystals are attached to the sheet-like morphology. On the other hand, the SEM image of BiCoO₃ revealed the aggregated particles with microscopic crystallinities on the sheet-like structure [34]. On the introduction of BiCoO₃ nanoparticles on the surface of the MOF-5 sheet, the layers of MOF-5 are fully intercalated with BiCoO₃ nanoparticles. In addition, the EDX analysis of the prepared samples was carried out to ensure the loading of BiCoO₃ on MOF-5. The results of EDX

indicate that the bismuth, cobalt, and oxygen element along with zinc are present on the surface of the MOF-5/BiCoO₃ composite, as seen in Figure 3d.

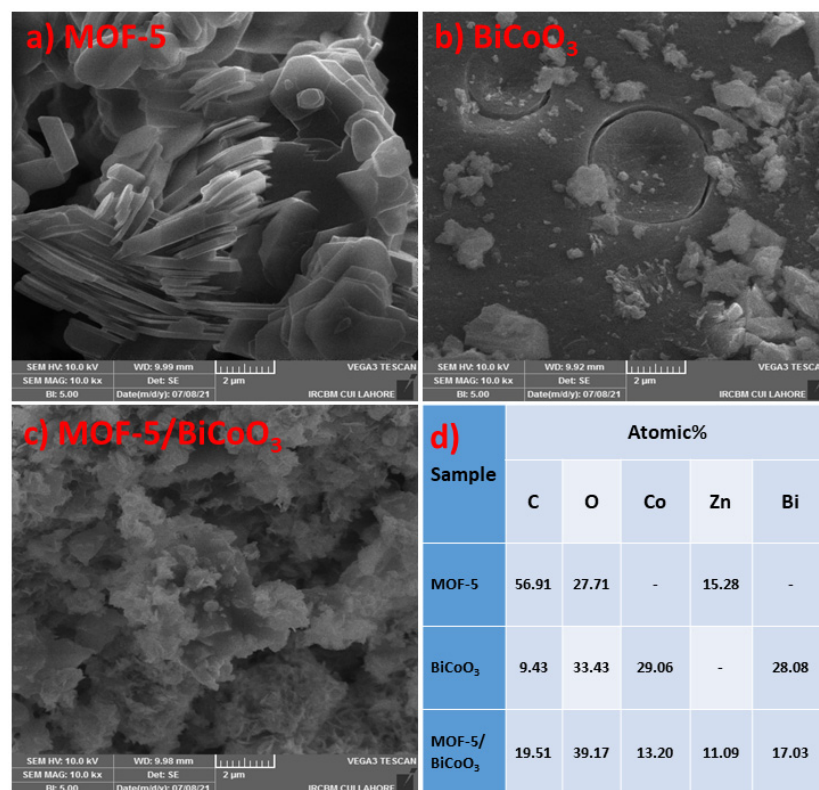


Figure 3. SEM morphology of MOF-5 (a); BiCoO₃ (b); MOF-5/BiCoO₃ composite (c); and EDX of prepared samples (d).

The functional groups on the surface of MOF-5, BiCoO₃, and MOF-5/BiCoO₃ composite were determined using Fourier transform infrared spectroscopy. The FTIR absorption spectra of MOF-5, BiCoO₃, and MOF-5/BiCoO₃ composite are recorded in the range of 500–4000 cm^{−1}, as shown in Figure 4. In MOF-5 spectra, the peak at 665 cm^{−1} appeared due to the formation of a tetrahedral coordinated Zn₄O cluster. The prominent peak at 825 cm^{−1} along with the peak from 1504 to 1507 cm^{−1} is associated with C-H stretching vibrations of aromatic rings, while the aliphatic asymmetric stretching of the C-H band appears at 2932 cm^{−1} [35]. The functional group of C=C stretching prominently appeared at 1580–1590 cm^{−1} [36]. The peak at 1661 cm^{−1} corresponds to the N-H vibrations due to the addition of the TEA capping agent during MOF-5 synthesis. The less intensified peak of O-H stretching vibrations is recorded in the range of 3200–3500 cm^{−1} [33]. In the BiCoO₃ spectrum, the band peak of Bi-O-Co can be observed at 571 cm^{−1}. The stretching vibration of the Co-O band in the Co₃O₄ phase appears at 825 cm^{−1}. The band peak appears at 1067 cm^{−1} corresponding to the Co-O-Co vibrations [25]. However, most of these peaks are disappeared or suppressed in the composite (MOF-5/BiCoO₃) spectra, which might be due to the formation of new heterojunctions between Bi-O-Zn and/or Co-O-Zn during the loading of semiconductor BiCoO₃ on MOF-5 surface. These new heterojunctions can be useful for the transfer of photoexcited electron-hole pairs.

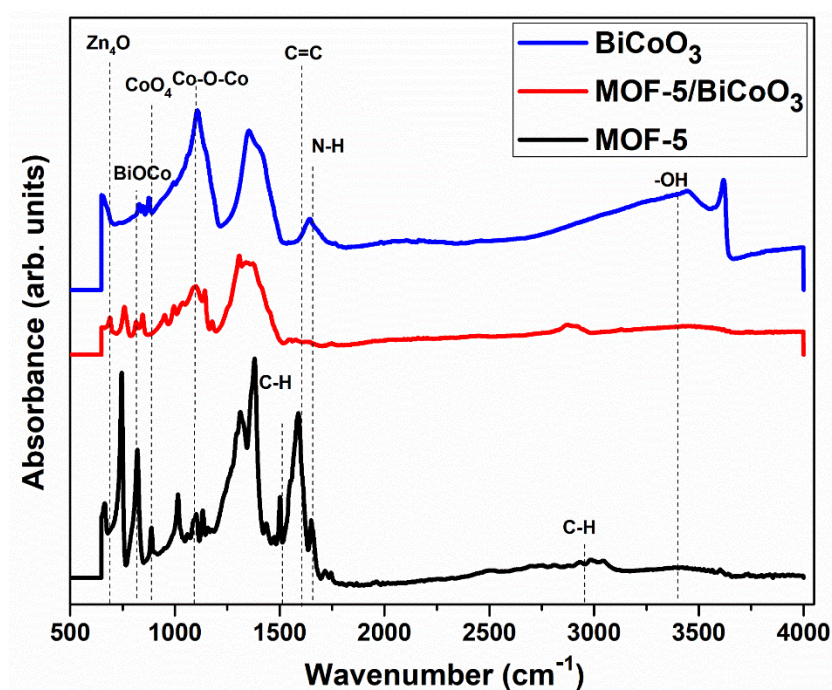


Figure 4. FTIR patterns of MOF-5, BiCoO₃ and MOF-5/BiCoO₃ composite.

The BET-specific surface area, pore size, and pore volume of MOF-5 and MOF-5/BiCoO₃ are represented in Figure 5. The highest specific surface area is observed up to 1062.44 m² g^{−1} for MOF-5/BiCoO₃ than pure MOF-5 (979.52 m² g^{−1}). The surface area of MOF-5/BiCoO₃ composite might be increased due to the introduction of semiconductor nanoparticles on MOF-5. Similarly, the surface area of MOF-5, with the addition of TEA as a capping agent during synthesis, is reported up to 1283.16 m² g^{−1} in the literature [35]. The pore volume and pore size are also higher for MOF-5/BiCoO₃ composite than pure MOF-5, as given in Figure 5. The higher surface area of MOF-5/BiCoO₃ composite provides more active sites for the adsorption of CR dye molecules on the surface of the photocatalyst.

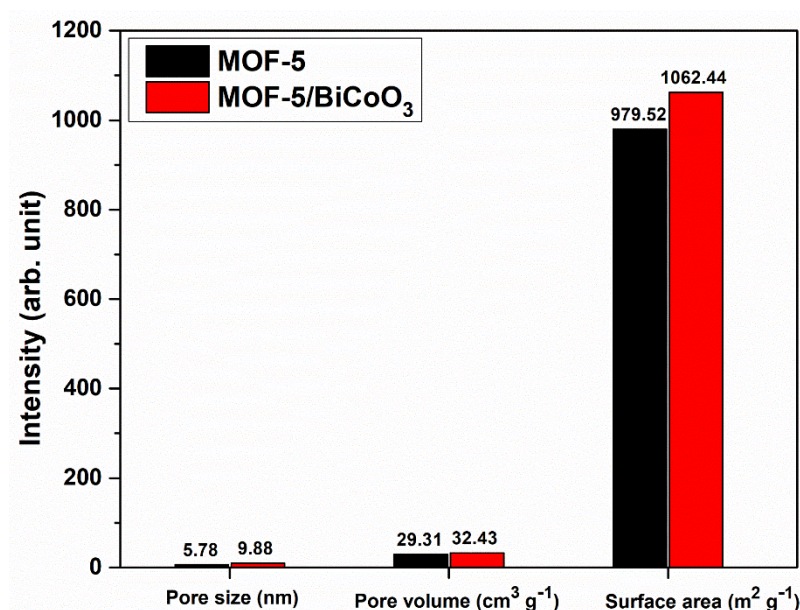


Figure 5. BET analysis of MOF-5 and MOF-5/BiCoO₃ composite.

Photoluminescence (PL) spectra are widely used to investigate the separation and/or transmission of charge carriers (e[−]/h⁺ pairs) toward semiconductor materials [9]. The

PL spectroscopy of MOF-5 and MOF-5/BiCoO₃ composite is carried out at the excitation wavelength of 579 nm. PL emission spectra of as-prepared samples are presented in Figure 6. It can be seen that the intensity of PL emission is higher for the MOF-5 sample, which indicates the fast recombination of charge carriers. Meanwhile, the PL emission is decreased significantly in the synthesis of MOF-5/BiCoO₃ composite as compared to pristine MOF-5. A significant decline in emissions for MOF-5/BiCoO₃ showed that the charge carriers are slowly recombined due to the formation of a new heterogeneous junction, as they can help out to improve the photocatalytic performance of modified MOF-5/BiCoO₃.

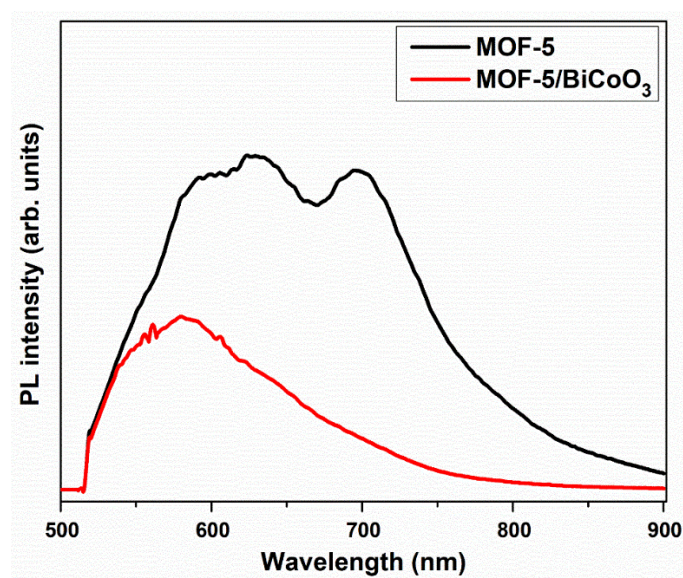


Figure 6. Photoluminescence (PL) spectra MOF-5 and MOF-5/BiCoO₃ composite.

3.2. Photocatalytic Degradation Performance and COD Removal

The photocatalytic performance of MOF-5 and MOF-5/BiCoO₃ photocatalysts was investigated for the degradation of CR dye molecules from simulated textile wastewater. The adsorptive-photocatalytic behavior of as-prepared samples was observed under dark (30 min) and UV-visible light (60 min) conditions. Initially, the adsorption-desorption equilibrium was achieved for prepared samples under dark conditions, which showed that MOF-5/BiCoO₃ composite has a fast adsorption rate of up to 41.1% as compared to pristine MOF-5 (32.7%) and BiCoO₃ (9.8%). Afterward, the photocatalytic performance for the degradation of CR was significantly enhanced up to 90 min using MOF-5/BiCoO₃ composite under UV-light irradiation, as shown in Figure 7a. The highest photocatalytic degradation (%) was achieved up to 99.6% using MOF-5/BiCoO₃ composite as compared to pristine MOF-5 (61.3%) and BiCoO₃ (47.3%). The formation of heterojunction within composite enhances the photocatalytic degradation of CR dye due to better light absorption, electron transmission, and suppression of charge carrier recombination (as discussed in Section 3.1). The results showed that the MOF-5/BiCoO₃ composite could act as an efficient and effective material to eliminate or degrade the CR dye molecules from the textile wastewater effluents, as shown in Figure 7b. In comparison to prepared samples, TiO₂ nanoparticles have been used as photocatalysts and achieved CR dye degradation up to 98% [37] and 70 % [38]. The mineralization of CR was verified by a COD test using photocatalysts. The COD removal (%) was measured using initial and final COD values. The results demonstrate that the highest COD removal (%) was determined up to 98.6% using MOF-5/BiCoO₃ as compared to 56.8% for MOF-5 and 48.1% for BiCoO₃ (see Figure 7c), which ensures that CR is properly degraded into smaller products as mentioned in Figure 7.

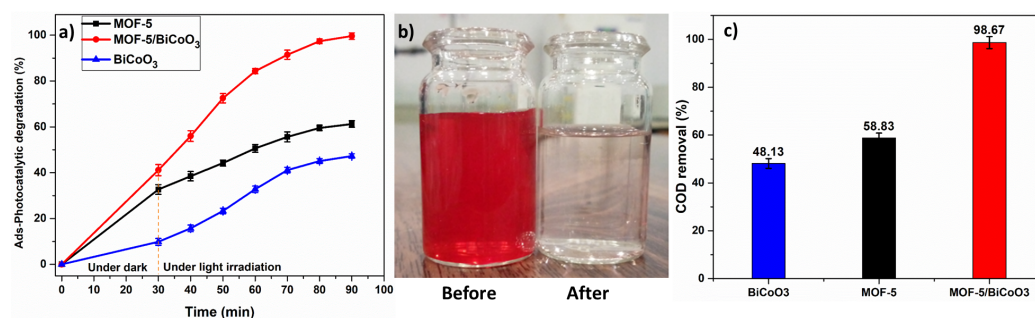
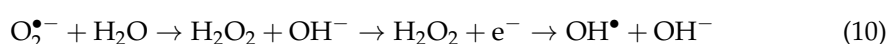
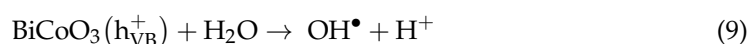
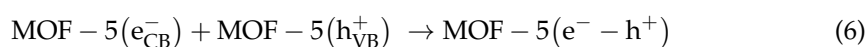
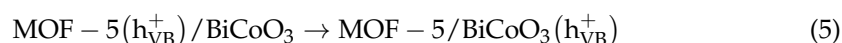
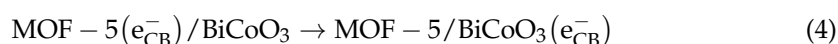
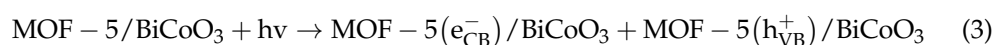


Figure 7. Adsorptive-photocatalytic degradation (%) (a); simulated textile wastewater before and after experiment using MOF-5/BiCoO₃ (b); and COD removal (%) of MOF-5, BiCoO₃, and MOF-5/BiCoO₃ composite (c).

3.3. Photocatalytic Reaction Mechanism

In MOF-5/ BiCoO₃ composite, the formation of heterogeneous structure between MOF-5 and BiCoO₃ nanoparticles enables it to absorb visible light radiations, which enhanced its photocatalytic degradation performance. During the photocatalytic process, the photons of light are absorbed by the electrons, present in the valence band of MOF-5, and then excited to the conduction band of MOF-5. Due to this fact, the holes are created in the corresponding valence band of MOF-5, as given in Equation (3). In MOF-5/ BiCoO₃ composite, BiCoO₃ provides the lower band positions of conduction (CB) and valence band (VB) as compared to MOF-5, and the face-to-face contact with MOF-5 formed a two-dimensional heterojunction structure [22]. The photoexcited electrons and holes of MOF-5 are transferred to the lower conduction band (Equation (4)) and lower valence band of BiCoO₃ (Equation (5)), respectively, through the interfaces between MOF-5 and BiCoO₃ nanoparticles, which reduces the recombination of charge carriers (electron-holes pair) of MOF-5 (Equation (6)). In order to determine the heterojunction type between MOF-5 and BiCoO₃, the energy for CB and VB of BiCoO₃ are calculated up to 0.7 eV and 2.9 eV, respectively, according to the literature [39]. Whereas, the CB and VB of MOF-5 are reported up to −0.58 and 3.28 eV, respectively [40]. According to the calculated (BiCoO₃) and literature values (MOF-5), the Type-I heterojunction is formed between MOF-5 and BiCoO₃ during the synthesis of MOF-5/BiCoO₃ composite.

The transferred photoexcited electrons in the conduction band of BiCoO₃ react with oxygen to reduce it to superoxide radicals (Equation (7)) and holes had a strong oxidizing ability to convert hydroxyl ions or water molecules into hydroxyl radicals (Equations (8) and (9)). The superoxide radicals also can convert water molecules into hydrogen peroxide, which is reduced into hydroxyl radicals, as shown in Equation (10). The reactive species of superoxide (O₂^{•−}) and hydroxyl (OH[•]) radicals react with CR dye molecules and degrade into smaller molecular products such as CO₂, H₂O, NH₄⁺, NO₃[−] and SO₄^{2−}, as seen in Equations (11) and (12). However, the possible route or mechanism of photocatalytic degradation of CR using MOF-5/BiCoO₃ composite is represented in Figure 8.



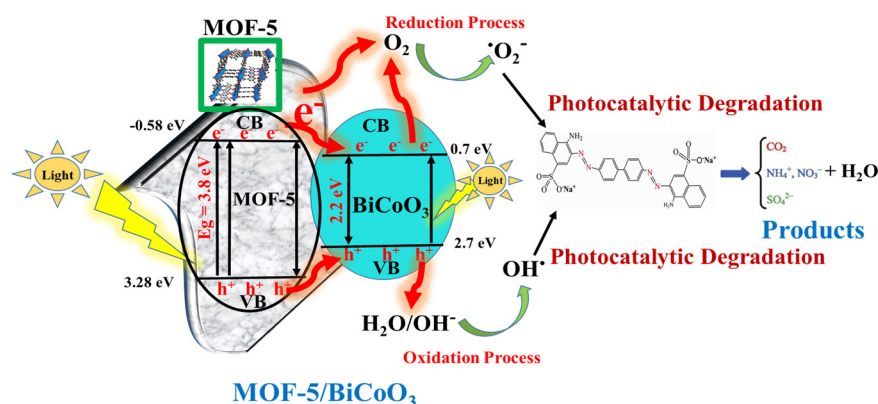
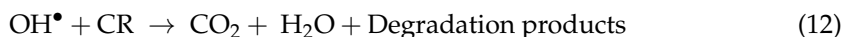
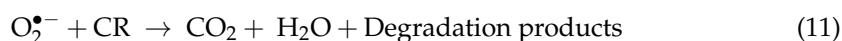


Figure 8. Photocatalytic mechanism of MOF-5/BiCoO₃ composite under light irradiation.

3.4. Radical Trapping and Reusability Experiment

The role of radicals in photocatalytic degradation of CR dye is evaluated by the use of radical scavengers. Three different scavengers are used to trap the radicals of superoxide, hydroxyl, and holes by the addition of BQ, IPA, and TEOA, respectively. The experimental results showed that photocatalytic degradation (%) of MOF-5/BiCoO₃ composite is significantly decreased by the addition of radical scavengers, as shown in Figure 9a. The photocatalytic performance is decreased from 99.5% to 50.9% with BQ scavengers, which depicts that the superoxide ($\text{O}_2^{\bullet -}$) radicals are the dominant radical species in the CR degradation process. In the addition of IPA, the CR photocatalytic degradation (%) is decreased up to 65.3%, as it can be observed that the trapping of OH^{\bullet} radicals also has a significant impact to decrease the photocatalytic performance of MOF-5/BiCoO₃ composite. Meanwhile, the CR degradation is slightly decreased on the introduction of TEOA, which demonstrate that holes are least reactive species in the photocatalytic degradation process.

The as-prepared samples are recycled for up to five cycles to evaluate their reusability in the photocatalytic degradation process. The photocatalytic performance of MOF-5/BiCoO₃ composite slightly declined with the recycling test, as shown in Figure 9b. The decline in performance is observed due to the unloading of nanoparticles during the washing process. However, more than 70% photocatalytic degradation of CR is achieved up to the fifth cycle, which confirmed that MOF-5/BiCoO₃ composite can be used as an efficient and economical to degrade CR dye molecules from textile wastewater effluents.

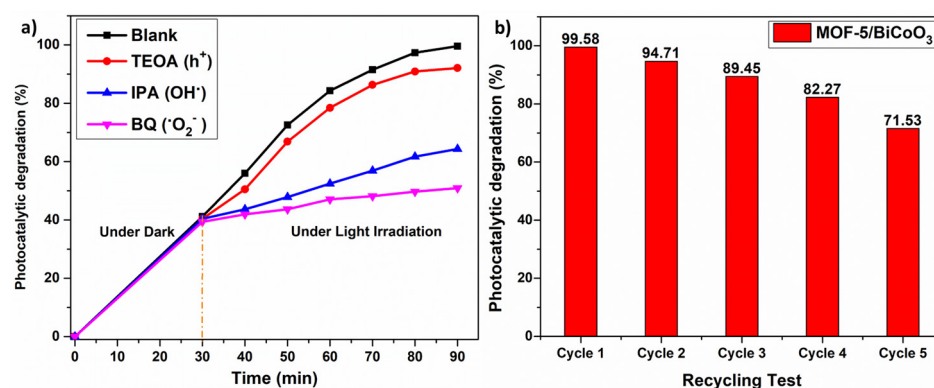


Figure 9. Role of radicals (a) and Reusability of MOF-5/BiCoO₃ composite in photocatalytic degradation process (b).

4. Conclusions

In this study, the MOF-5-based BiCoO₃ composite was synthesized using one pot hydrothermal process. The as-prepared samples were characterized to evaluate their intrinsic properties such as crystallinity, surface area, morphology, functional groups at surface sites, and recombination of charge carriers using different analytical techniques. The photocatalytic degradation rate of CR was achieved up to 99.6% using MOF-5/BiCoO₃ composite as compared to MOF-5 (61.3%) and BiCoO₃ (47.3%). The COD removal (%) was determined at about 98.6% using MOF-5/BiCoO₃ composite, which confirms the mineralization of CR into smaller products such as CO₂, H₂O, NO₃[−], NH₄⁺, and SO₄^{−2}. During the photocatalytic process, the main reactive species such as O₂^{•−} and OH[•] radicals are more dominant in the degradation of CR molecules. The MOF-5/BiCoO₃ composite is a highly stable, effective, efficient, and economical photocatalyst, as it can be used for up to five cycles and achieve more than 70% photocatalytic degradation of CR. Hence, the results suggest that the synthesis of MOF-5/BiCoO₃ composite offers an enlightened approach to designing highly effective, efficient, and economical heterostructure photocatalysts for the treatment of organic dyes from textile wastewater.

Author Contributions: Conceptualization, A.U.K. and M.A.; methodology, B.S. and M.A.; formal analysis, B.S. and T.F.; investigation, B.S. and T.F.; resources, A.U.K. and N.A.Q.; data curation, A.A.; writing—original draft preparation, B.S. and T.F.; writing—review and editing, A.A. and T.F.; visualization, N.A.Q.; supervision, A.U.K. and M.A.; project administration, A.U.K.; funding acquisition, A.U.K. All authors have read and agreed to the published version of the manuscript.

Funding: This research was funded by Pak-US Science & Technology Cooperation Program under HEC-Pakistan, Phase –VI, entitled “A Sustainable Point-of-Use filtration Unit for Treating Pesticide Contaminated Ground water” (PAK-US/HEC/2015/12).

Institutional Review Board Statement: Not applicable.

Informed Consent Statement: Not applicable.

Data Availability Statement: All data is included in the text of the manuscript.

Acknowledgments: The authors acknowledge the support provided by the Department of Chemical Engineering, COMSATS University Islamabad, Lahore Campus Pakistan. The authors want to thank Fahad Rehman for his permission to use the resources of the Microfluidic Research Lab. We would like to thank Engr. Tahir Saif for his technical support for characterization results.

Conflicts of Interest: The authors declare no conflict of interest.

Abbreviation

MOF	Metal Organic Framework
CR	Congo red
BQ	Benzene Quinone
TEOA	Triethanolamine (TEOA),
IPA	Isopropanol (IPA)
COD	Chemical Oxygen Demand

References

1. Zhou, F.Y.; Mao, J.N.; Peng, X.L.; Hong, B.; Xu, J.C.; Zeng, Y.X.; Han, Y.B.; Ge, H.L.; Wang, X.Q. Magnetically Separable Ni/g-C₃N₄ Nanocomposites for Enhanced Visible-Light Photocatalytic Degradation of Methylene Blue and Ciprofloxacin. *Diam. Relat. Mater.* **2022**, *126*, 109070. [CrossRef]
2. Iqbal, J.; Shah, N.S.; Sayed, M.; Khan, N.; Imran, M.; Ali, J.; Ul, Z.; Khan, H.; Gamal, A.; Hussien, S. Nano-Zerovalent Manganese/Biochar Composite for the Adsorptive and Oxidative Removal of Congo-Red Dye from Aqueous Solutions. *J. Hazard. Mater.* **2021**, *403*, 123854. [CrossRef]
3. Tabasum, B.; Dhagale, P.R.; Nitnaware, K.M.; Nikule, H.A.; Nikam, T.D. New Chemical Products Formation from Textile Dye Degradation, Chitinolytic and Antioxidant Activity in New Strain Nbpc5-18 of Cellulosimicrobium Sp. TH-20. *J. Environ. Chem. Eng.* **2019**, *7*, 103114. [CrossRef]

4. Suleman, M.; Zafar, M.; Ahmed, A.; Rashid, M.U.; Hussain, S.; Razzaq, A.; Mohidem, N.A.; Fazal, T.; Haider, B.; Park, Y.K. Castor Leaves-Based Biochar for Adsorption of Safranin from Textile Wastewater. *Sustainability* **2021**, *13*, 6926. [\[CrossRef\]](#)
5. Singh, S.; Perween, S.; Ranjan, A. Dramatic Enhancement in Adsorption of Congo Red Dye in Polymer-Nanoparticle Composite of Polyaniline-Zinc Titanate. *J. Environ. Chem. Eng.* **2021**, *9*, 105149. [\[CrossRef\]](#)
6. Koochi, P.; Rahbar-kelishami, A.; Shayesteh, H. Efficient Removal of Congo Red Dye Using Fe₃O₄/NiO Nanocomposite: Synthesis and Characterization. *Environ. Technol. Innov.* **2021**, *23*, 101559. [\[CrossRef\]](#)
7. Fazal, T.; Faisal, A.; Mushtaq, A.; Hafeez, A.; Javed, F.; Alaud Din, A.; Rashid, N.; Aslam, M.; Rehman, M.S.; Rehman, F. Macroalgae and Coal-Based Biochar as a Sustainable Bioresource Reuse for Treatment of Textile Wastewater. *Biomass Convers. Biorefinery* **2019**, *11*, 1491–1506. [\[CrossRef\]](#)
8. Ahmad, R.; Ahmad, Z.; Ullah, A.; Riaz, N.; Aslam, M.; Kim, J. Photocatalytic Systems as an Advanced Environmental Remediation: Recent Developments, Limitations and New Avenues for Applications. *J. Environ. Chem. Eng.* **2016**, *4*, 4143–4164. [\[CrossRef\]](#)
9. Fazal, T.; Razzaq, A.; Javed, F.; Hafeez, A.; Rashid, N.; Amjad, U.S.; Ur Rehman, M.S.; Faisal, A.; Rehman, F. Integrating Adsorption and Photocatalysis: A Cost Effective Strategy for Textile Wastewater Treatment Using Hybrid Biochar-TiO₂ Composite. *J. Hazard. Mater.* **2020**, *390*, 121623. [\[CrossRef\]](#) [\[PubMed\]](#)
10. Sharma, M.; Yadav, A.; Mandal, M.K.; Dubey, K.K. TiO₂ Based Photocatalysis: A Valuable Approach for the Removal of Pharmaceuticals from Aquatic Environment. *Int. J. Environ. Sci. Technol.* **2022**, *2010*. [\[CrossRef\]](#)
11. Samsudin, M.F.R.; Sufian, S.; Hameed, B.H. Epigrammatic Progress and Perspective on the Photocatalytic Properties of BiVO₄-Based Photocatalyst in Photocatalytic Water Treatment Technology: A Review. *J. Mol. Liq.* **2018**, *268*, 438–459. [\[CrossRef\]](#)
12. Leichtweis, J.; Silvestri, S.; Carissimi, E. New Composite of Pecan Nutshells Biochar-ZnO for Sequential Removal of Acid Red 97 by Adsorption and Photocatalysis. *Biomass Bioenergy* **2020**, *140*, 105648. [\[CrossRef\]](#)
13. Zhang, T.; Li, W.; Guo, Q.; Wang, Y.; Li, C. Preparation of a Heterogeneous Catalyst CuO-Fe₂O₃/CTS-ATP and Degradation of Methylene Blue and Ciprofloxacin. *Coatings* **2022**, *12*, 559. [\[CrossRef\]](#)
14. Yang, J.; Luo, X. Ag-Doped TiO₂ Immobilized Cellulose-Derived Carbon Beads: One-Pot Preparation, Photocatalytic Degradation Performance and Mechanism of Ceftriaxone Sodium. *Appl. Surf. Sci.* **2021**, *542*, 148724. [\[CrossRef\]](#)
15. Chen, X.; Zhang, Y.; Kong, X.; Yao, K.; Liu, L.; Zhang, J.; Guo, Z.; Xu, W.; Fang, Z.; Liu, Y. Photocatalytic Performance of the MOF-Coating Layer on SPR- Excited Ag Nanowires. *ACS Omega* **2021**, *6*, 2882–2889. [\[CrossRef\]](#) [\[PubMed\]](#)
16. Tayebi, M.; Kolaei, M.; Tayyebi, A.; Masoumi, Z.; Belbasi, Z.; Lee, B.K. Reduced Graphene Oxide (RGO) on TiO₂ for an Improved Photoelectrochemical (PEC) and Photocatalytic Activity. *Sol. Energy* **2019**, *190*, 185–194. [\[CrossRef\]](#)
17. Younis, S.A.; Serp, P.; Nassar, H.N. Photocatalytic and Biocidal Activities of ZnTiO₃ Oxynitride Heterojunction with MOF-5 and g-C₃N₄: A Case Study for Textile Wastewater Treatment under Direct Sunlight. *J. Hazard. Mater.* **2020**, *410*, 124562. [\[CrossRef\]](#)
18. Silvestri, S.; Gonçalves, M.G.; Da Silva Veiga, P.A.; Matos, T.T.D.S.; Peralta-Zamora, P.; Mangrich, A.S. TiO₂ Supported on Salvinia Molesta Biochar for Heterogeneous Photocatalytic Degradation of Acid Orange 7 Dye. *J. Environ. Chem. Eng.* **2019**, *7*, 102879. [\[CrossRef\]](#)
19. Wang, C.C.; Yi, X.H.; Wang, P. Powerful Combination of MOFs and C₃N₄ for Enhanced Photocatalytic Performance. *Appl. Catal. B Environ.* **2019**, *247*, 24–48. [\[CrossRef\]](#)
20. Mo, Z.; Tai, D.; Zhang, H.; Shahab, A. A Comprehensive Review on the Adsorption of Heavy Metals by Zeolite Imidazole Framework (ZIF-8) Based Nanocomposite in Water. *Chem. Eng. J.* **2022**, *443*, 136320. [\[CrossRef\]](#)
21. Valero-Romero, M.J.; Santaclara, J.G.; Oar-Arteta, L.; van Koppen, L.; Osadchii, D.Y.; Gascon, J.; Kapteijn, F. Photocatalytic Properties of TiO₂ and Fe-Doped TiO₂ Prepared by Metal Organic Framework-Mediated Synthesis. *Chem. Eng. J.* **2019**, *360*, 75–88. [\[CrossRef\]](#)
22. Yao, T.; Tan, Y.; Zhou, Y.; Chen, Y.; Xiang, M. Preparation of Core-Shell MOF-5/Bi₂WO₆ Composite for the Enhanced Photocatalytic Degradation of Pollutants. *J. Solid State Chem.* **2022**, *308*, 122882. [\[CrossRef\]](#)
23. Lu, G.; Chu, F.; Huang, X.; Li, Y.; Liang, K.; Wang, G. Recent Advances in Metal-Organic Frameworks-Based Materials for Photocatalytic Selective Oxidation. *Coord. Chem. Rev.* **2022**, *450*, 214240. [\[CrossRef\]](#)
24. Sun, W.; Wang, W.; Chen, D.; Zhang, G.; Cheng, Z.; Wang, Y. First-Principles Investigation on Tunable Electronic Properties and Magnetism by Polarization in PbTiO₃/BiFeO₃ 2D Ferroelectric Heterostructures. *J. Mater. Chem. C* **2019**, *7*, 463–473. [\[CrossRef\]](#)
25. Lopes, J.A.; Sabino, E.B.; Raimundo, R.A.; Ribeiro, D. (Bi₁₃Co₁₁)Co₂O₄₀-Co₃O₄ Composites: Synthesis, Structural and Magnetic Properties. *J. Alloys Compd.* **2021**, *852*, 156991. [\[CrossRef\]](#)
26. Liu, H.; Li, X.; Peng, C.; Zhu, L.; Zhang, Y.; Cheng, H.; Cui, J.; Wu, Q.; Lu, Y. Activating the Lattice Oxygen in (Bi_{0.5}Co_{0.5})₂O₃ by Vacancy Modulation for Efficient Electrochemical Water Oxidation. *J. Mater. Chem. A* **2020**, *8*, 13150–13159. [\[CrossRef\]](#)
27. Pan, C.; Wang, Z.; Lou, Y.; Zhang, Y.; Dong, Y. The Construction of a Wide-Spectrum-Responsive and High-Activity Photocatalyst, Bi₂₅CoO₄₀, via the Creation of Large External Dipole of Large External Dipoles. *J. Mater. Chem. A* **2021**, *3*, 3616–3627. [\[CrossRef\]](#)
28. Qin, X.; Qiang, T.; Chen, L.; Wang, S. Construction of 3D N-CQD/MOF-5 Photocatalyst to Improve the Photocatalytic Performance of MOF-5 by Changing the Electron Transfer Path. *Microporous Mesoporous Mater.* **2021**, *315*, 110889. [\[CrossRef\]](#)
29. Rodríguez, N.A.; Parra, R.; Grela, M.A. Structural Characterization, Optical Properties and Photocatalytic Activity of MOF-5 and Its Hydrolysis Products: Implications on Their Excitation Mechanism. *RSC Adv.* **2015**, *5*, 73112–73118. [\[CrossRef\]](#)
30. Si, Y.; Li, Y.; Zou, J.; Xiong, X.; Zeng, X.; Zhou, J. Photocatalytic Performance of a Novel MOF/BiFeO₃ Composite. *Materials* **2017**, *10*, 1161. [\[CrossRef\]](#)

31. Zhao, H.; Song, H.; Chou, L. Nickel Nanoparticles Supported on MOF-5: Synthesis and Catalytic Hydrogenation Properties. *Inorg. Chem. Commun.* **2012**, *15*, 261–265. [[CrossRef](#)]
32. Chen, A.; Zhang, J.; Zhou, Y.; Tang, H. Preparation of a Zinc-Based Metal–Organic Framework (MOF-5)/BiOBr Heterojunction for Photodegradation of Rhodamine B. *React. Kinet. Mech. Catal.* **2021**, *134*, 1003–1015. [[CrossRef](#)]
33. Hajiashra, S.; Motakef, N. Preparation and Evaluation of ZnO Nanoparticles by Thermal Decomposition of MOF-5. *Heliyon* **2019**, *5*, e02152. [[CrossRef](#)]
34. Ramachandran, T.; Rajeevan, N.E.; Pradyumnan, P.P. Enhanced Thermoelectric Properties of BiCoO₃ by Nickel Substitution. *Mater. Sci. Appl.* **2013**, *4*, 816–821. [[CrossRef](#)]
35. Reza, M.; Negar, M.; Ashouri, M.F. Nitrate Adsorption from Aqueous Solution by Metal–Organic Framework MOF-5. *Iran. J. Sci. Technol. Trans. A Sci.* **2019**, *43*, 443–449. [[CrossRef](#)]
36. Savic, M.; Marjanovi, B.; Zaso, B.A.; Stojadinovi, S.; Gordana, Ć. Novel Microporous Composites of MOF-5 and Polyaniline with High Specific Surface Area. *Synth. Met.* **2020**, *262*, 116348. [[CrossRef](#)]
37. Erdemoğlu, S.; Aksu, S.K.; Sayilkan, F.; Izgi, B.; Asiltürk, M.; Sayilkan, H.; Frimmel, F.; Güçer, Ş. Photocatalytic Degradation of Congo Red by Hydrothermally Synthesized Nanocrystalline TiO₂ and Identification of Degradation Products by LC-MS. *J. Hazard. Mater.* **2008**, *155*, 469–476. [[CrossRef](#)]
38. Harun, N.H.; Rahman, M.N.A.; Kamarudin, W.F.W.; Irwan, Z.; Muhammad, A.; Akhir, N.E.F.M.; Yaafar, M.R. Photocatalytic Degradation of Congo Red Dye Based on Titanium Dioxide Using Solar and Uv Lamp. *J. Fundam. Appl. Sci.* **2018**, *10*, 832–846. [[CrossRef](#)]
39. Mousavi, M.; Habibi-Yangjeh, A.; Abitorabi, M. Fabrication of Novel Magnetically Separable Nanocomposites Using Graphitic Carbon Nitride, Silver Phosphate and Silver Chloride and Their Applications in Photocatalytic Removal of Different Pollutants Using Visible-Light Irradiation. *J. Colloid Interface Sci.* **2016**, *480*, 218–231. [[CrossRef](#)]
40. Zhai, B.; Chen, Y.; Li, J.; Liang, Y. Two-Dimensional Composite (BiOCl/GO/MOF-5) by Ultrasonic-Assisted Solvothermal Synthesis with Enhanced Photocatalytic Activity. *Micro Nano Lett.* **2020**, *15*, 149–154. [[CrossRef](#)]